



Cite this: *Phys. Chem. Chem. Phys.*,
2020, **22**, 14941

Controlling the nanoscale friction by layered ionic liquid films[†]

Rong An, ^{*ab} Xiuhua Qiu,^a Faiz Ullah Shah, ^c Kristina Riehemann^b and Harald Fuchs^{*ab}

The nanofriction coefficient of ionic liquids (ILs), 1-butyl-3-methylimidazolium tetrafluoroborate ($[\text{BMIM}][\text{BF}_4]$) and 1-butyl-3-methylimidazolium hexafluorophosphate ($[\text{BMIM}][\text{PF}_6]$), on the surfaces of mica and graphite was investigated using atomic force microscopy (AFM). A pronounced layered spatial distribution was found in the IL film formed on the solid substrates and can be divided into 3 well distinguishable regions exhibiting different physical properties with increasing distance from the substrate. We found that the friction coefficient (μ) increases monotonically as the layering thickness decreases, no matter what the thickness of the bulk IL is. This suggests that the layering assembled IL at solid surfaces is more important than the bulk phase in determining the magnitude of the nanoscale friction. The increase in the friction coefficient as the layering thickness decreases is most likely attributed to the assembled ordered IL layers closer to the substrate surfaces having a greater activation barrier for unlocking the surfaces to allow shear.

Received 22nd April 2020,
Accepted 22nd June 2020

DOI: 10.1039/d0cp02146f

rsc.li/pccp

1. Introduction

Ionic liquids (ILs) are salts made of cations and anions which usually exist in liquid state at room temperature. ILs were initially demonstrated as high performance versatile synthetic lubricants in 2001.^{1,2} ILs based lubricants have many advantages over the conventional oil because of their unique physicochemical properties such as low vapor pressure, high chemical and thermal stabilities, nonflammability, excellent thermal conductivity, high ionic conductivity, and molecular designability.³ Typically, ILs possess inherent polarity for strong surface adsorption *via* a combination of van der Waals, electrostatic, and hydrogen-bonding interactions.⁴

An ideal IL layer adsorbed at sliding solid interfaces is expected to avoid corrosion of the surfaces, support high loads and prevent direct surface-to-surface contact, and thus offering an anti-wear ability as well as reduced friction. The ability of adsorbate IL layers to 'wet' the solid surface depends on the competition^{5,6} between the IL-solid and IL-IL intermolecular

forces. The strength of interactions of ILs with the underlying solid surface determines the dynamic properties and nanostructures of the near-surface ILs, which is apparently different from that of the bulk.^{7,8} For example, an ordered crystalline phase of ILs was found to coexist with the mobile liquid phase on a graphite surface, which is caused by a comparable strength of the IL-substrate and IL-IL interactions.⁹ Extended layering structures of ILs on solid surfaces were observed in force-distance profiles using atomic force microscopy (AFM), which is a consequence of both the adjacent IL-solid and bulk IL-IL interaction strength.^{10,11} The similar extended layering packed ions in ILs on mica surfaces were later found to be the result of an ion exchange between K^+ and the cations of ILs on the mica surface.¹²

The strength of IL-solid interactions is more pronounced to influence the ILs behavior at the solid surface, however, the strength decreases as the distance from the solid substrate increases.¹³ We have previously confirmed this effect in the adsorbate nanofriction in polymer films, where thick polymer films coated solid substrates possess nanofriction properties approaching those of the bulk polymer.¹⁴ In another findings with a surface force balance at a microscale, an increased friction in 1-butyl-1-methylpyrrolidinium bis[(trifluoromethane)sulfonyl]imide confined between two mica sheets was observed as the number of ion layers decreases. The authors attributed the increased friction coefficient with the decreased ion layer to the greater degree of interlocking of the layers for a thinner layer: the layers closer to the mica surfaces are more ordered, with a greater ion excess concentration, resulting in a stronger 'inter-layer attraction for the same value of contact area and a greater activation barrier for unlocking the surfaces to allow shear'.¹⁵

^a Herbert Gleiter Institute of Nanoscience, Department of Materials Science and Engineering, Nanjing University of Science and Technology, Nanjing 210094, P. R. China. E-mail: ran@njust.edu.cn, fuchsh@uni-muenster.de; Fax: +86-025-84303400; Tel: +86-025-84303400

^b Center for Nanotechnology (CeNTech), Institute of Physics, Westfälische Wilhelms-Universität Münster, 48149 Münster, Germany

^c Chemistry of Interfaces, Luleå University of Technology, SE 971 87 Luleå, Sweden

[†] Electronic supplementary information (ESI) available: AFM topographical, phase images and corresponding cross-sectional profiles, Topographic images of BB3-4-M before and after nano-shaving with a normal force of ~ 300 nN, approaching force *vs.* distance curves measured by glass colloidal probes, friction force *vs.* applied normal load plots, torsional resonance spectra, and high-resolution XPS spectra. See DOI: 10.1039/d0cp02146f

Recently, the confined ILs were observed to exhibit a dramatic change towards a solid-like phase with a tungsten AFM tip in vacuum.¹⁶ The metallic nature of the confining materials facilitates this liquid-to-solid phase shift. In detail, the ILs start to experience solid phase shift at a greater distance to the more metallic substrate, while the occurrence of this shift on a less metallic surface is only possible when ILs are closer. The formed solid phase ILs were suggested to reduce nanoscale friction by the prevention of direct substrate-to-substrate contact. This underlines that the near-surface IL layer at nanoscale is peculiar and leads to significantly different behavior from what is observed in the bulk. Here some pertinent questions arise about IL-solid systems in the context of nanoscale friction: is the contribution to nanofriction mainly from, the near-surface IL or the bulk phase? and how is this nanofriction susceptible to the distance from the solid substrate?

The distance to the solid substrate can be modeled as the IL thickness at solid interfaces. A larger thickness corresponds to the IL ions further away from the substrate, which could be considered as the bulk phase of the IL. The thickness of IL layer was thus varied in this work to examine the change in the magnitude of nanoscale friction as a function of distance from the solid substrate. To answer the above questions, we systematically performed AFM experiments to investigate the nanoscale friction in two ILs films—1-butyl-3-methylimidazolium tetrafluoroborate ([BMIM][BF₄], abbreviated as BB) and 1-butyl-3-methylimidazolium hexafluorophosphate ([BMIM][PF₆], abbreviated as BP) on both mica and highly oriented pyrolytic graphite (HOPG) planar substrates.

2. Experimental

2.1. Materials

Mica and highly oriented pyrolytic graphite (HOPG) substrates were purchased from VWR International and MikroMasch respectively. The ILs, 1-butyl-3-methylimidazolium tetrafluoroborate

([BMIM][BF₄], purity $\geq 98\%$) and 1-butyl-3-methylimidazolium hexafluorophosphate ([BMIM][PF₆], purity $\geq 97\%$) were purchased from Sigma-Aldrich and used as received. Dodecenyl succinic anhydride (DDSA) and benzylidimethylamine (BDMA) were received from Sinopharm Chemical Reagent Co., Ltd, and Araldite Resin CY212 (CY212) was obtained from Sigma-Aldrich. The AFM tips that were used in friction and surface morphology measurements were respectively DNP-10 and RTESP-300 tips from Bruker. The NSC35 tipless Cr-Au coated cantilevers were purchased from Mikromasch, and the borosilicate glass microspheres were from SPI Supplies.

2.2. Preparation of ILs films on mica and HOPG surfaces

The ILs, [BMIM][BF₄] and [BMIM][PF₆], were dissolved in ethanol to yield IL solutions with different concentrations, *i.e.*, 10^{-5} , 10^{-4} , 10^{-3} mL ILs per mL ethanol. The as-prepared IL solutions were respectively dropped on mica and HOPG substrates (area = $1 \times 1 \text{ cm}^2$) with varying volume and then allowed the ethanol to completely evaporate in vacuum at 35°C for 12 h. After evaporation of ethanol, ILs films of different thicknesses were obtained (see Table 1).

2.3. Friction force measurements

Friction force measurements were performed on a dimension icon atomic force microscopy (AFM, Bruker) in contact mode at ambient conditions. V-shaped Si₃N₄ cantilevers (DNP-10, A tip, tip radius = 20 nm) with a nominal spring constant of 0.35 N m^{-1} were employed throughout the friction measurements, and the scan rate was 2 Hz. The normal spring constant of each AFM tip was calibrated using deflection sensitivity of the supported cantilever to transform the normal load signals (in V) into true normal load (in N). The measurements were performed under varied applied loads, using lateral force images derived from trace and retrace tracks of $5 \mu\text{m} \times 5 \mu\text{m}$ under the tip at a 90° scan angle to the cantilever long axis. The average lateral force, given in terms of an output voltage signal (half-difference of the average lateral deflection signal on the photodetector of

Table 1 ILs films on solid (M = mica, H = HOPG) surfaces

	Mica, 1 cm^2		HOPG, 1 cm^2	
	BB ^b	BP ^c	BB	BP
10^{-5} mL IL per mL ethanol, 1 μL	BB5-1-M	BP5-1-M	BB5-1-H	BP5-1-H
10^{-4} mL IL per mL ethanol, 1 μL	BB4-1-M	BP4-1-M	BB4-1-H	BP4-1-H
10^{-3} mL IL per mL ethanol, 1 μL	BB3-1-M	BP3-1-M	BB3-1-H	BP3-1-H
10^{-3} mL IL per mL ethanol, 4 μL	BB3-4-M	BP3-4-M	BB3-4-H	BP3-4-H
10^{-3} mL IL per mL ethanol, 8 μL	BB3-8-M	BP3-8-M	BB3-8-H	BP3-8-H

^a The illustrations represent the IL films on solid surfaces with varying film thicknesses (t_A , see Sections 2.4 and 3.1) after the evaporation of ethanol. ^b BB = [BMIM][BF₄]. ^c BP = [BMIM][PF₆].

the forward and reverse traces, in V) was then transformed into a true friction force (in N) from the torsion of the cantilever.¹⁷ The friction coefficient, μ , defined as the constant of proportionality between the measured nanoscale friction and applied load, is the conventional way of quantifying the friction. The torsional resonance frequency was obtained using a probe with similar parameters as the DNP-10, but with a rectangular cantilever.

It is noteworthy that majority of previous reports in IL-solid systems were conducted under ambient conditions. Our frictional experiments were also performed at ambient temperature (~ 298 K), with a humidity of $\sim 55\%$. In a recent findings, the humidity was found to strongly increase the resistance of the IL layers to be squeezed-out, without changing significantly their corresponding thicknesses and friction coefficients. The beneficial effect of water on resisting the “squeeze-out” of IL layers, leads to an extension of the loading range. This is interesting for applications with hygroscopic ILs and lubricated systems which are never perfectly insulated from ambient moisture.¹⁸ We focus on the dependence of nanoscale friction coefficient on the layering thickness of ILs, so we measured the layering thickness and friction forces immediately after the IL-solid samples were prepared, to prevent their long-time exposure to the moisture.

2.4. Measurements of the apparent film thickness of ILs on mica and HOPG surfaces

We approximated the difference in the approaching force-distance curve between the jump-in position of the piezo and the zero-force point as the apparent thickness of the IL film on surfaces (t_A) using AFM colloidal probes.^{8,19,20} The apparent thickness of the IL film includes the ILs near the substrate and the bulk ILs (see Section 3.1). The AFM colloidal probes were obtained by attaching borosilicate glass microspheres (20 μm in dimension) to tipless Cr-Au coated cantilevers (Cantilever A with a length of 110 μm) with epoxy glue (DDSA:BDMA: CY212 = 10:1:10 in volume ratio), monitored through the optical microscope of the AFM.

2.5. Nanostructural characterization of ILs films on mica and HOPG surfaces

The assembled IL layers cannot be observed easily in contact mode, so most previous reports observed the extended layering in tapping mode with AFM, which does not disturb the liquid molecular layers.^{12,21–24} Thus, in this work, surface morphologies of IL films on the surfaces were obtained using tapping mode AFM with RTESP-300 silicon probes. The thicknesses of the assemble IL layers on mica/HOPG surfaces were determined by peak-to-valley distances which were obtained by averaging at least 10 profiles per topographic image at three separate locations for each of the samples used. However, in the determination of the layering thickness, we excluded the inhomogeneous IL droplets on the solid substrates. Because the droplets are similar to the bulk ILs, which is not playing a dominant role in the nanoscale friction coefficient at IL-solid interfaces in the present work (see Section 3.3).

X-ray photoelectron energy spectra (XPS) were recorded using a Thermo VG Scientific X-ray photoelectron spectrometer with a monochromatic Al $K\alpha$ X-ray. The energy scale and transmission function of the analyzer are calibrated using standard gold, silver and copper sample. XPS depth profiles were utilized to analyze the element distribution of ILs at varying distances from the solid substrates.

3. Results and discussion

3.1. Layering assembled IL films at solid surfaces

To explore the changes in nanoscale friction due to the variations in the film thickness of ILs at solid surfaces, well-defined BB and BP films have been yielded through drop-casting IL-ethanol dispersions and drying them in vacuum. AFM height and phase shift images were used to characterize the IL films deposited on mica and HOPG surfaces. Fig. 1a and Fig. S1 (ESI[†]) show the local morphologies of the resulted IL films. In the case of BB3-4-M where the IL film formed after a complete evaporation of ethanol by using 10⁻³ mL [BMIM][BF₄] IL per mL ethanol (4 μL) on the mica surface, we clearly observed the extended layering structure with a thickness of ~ 2.1 nm, as shown in Fig. 1a and c. As for the other cases in AFM topographic images shown in Fig. S1 (ESI[†]), some of IL drops resided on the layering assembled IL films, forming drop-on-layer structures. Some well-growing IL films appeared to stack on top of the networking assembled IL layers, especially in the case of BP5-1-M. We also noted that BP3-8-H, BP3-1-H, and BP4-1-H exhibited sharp edges in the assembled layers parallel to each other at some preferred orientation, which is most probably due to the HOPG lattice-matching effect and/or restriction of the underlying HOPG terraces.^{25,26} The assembled IL layers crossing over HOPG steps were also observed.

The phase shift image reflects the mechanical response (the elasticity) of the sample.²⁷ The varying phase contrast in a given IL-solid system correspond to different structures of IL layers (Fig. S1, ESI[†]), where the extend ordered layering structure of ILs decayed at a greater distance from the underlying solid surface. Thus, it is understandable that the phase contrast varies in a given IL-solid system. Comparing the topographic and phase images in Fig. 1a and b, the extended layer showed a completely different brightness from the lower step area in the phase images, indicating two different local elasticities between them. This observed elasticity difference suggested the lower part in AFM topographic image is the surface of the substrate, rather than the IL layers adsorbed on the substrate. To check if the lower step areas in the topographic images are the underlying substrate, we took the BB3-4-M as an example, and did a 5 $\mu\text{m} \times 5 \mu\text{m}$ range scan to obtain a topographic image in tapping mode (left panel, Fig. S2, ESI[†]), and then performed nano-shaving in contact mode with a normal force of ~ 300 nN. Afterwards, another 5 $\mu\text{m} \times 5 \mu\text{m}$ scan in tapping mode (right panel, Fig. S2, ESI[†]) was made. As expected, no scratching (no removal of any layers) was observed in the lower part, while some of the IL layers were removed during the scan, confirming that the lower part is the surface of the substrate. Thus, the

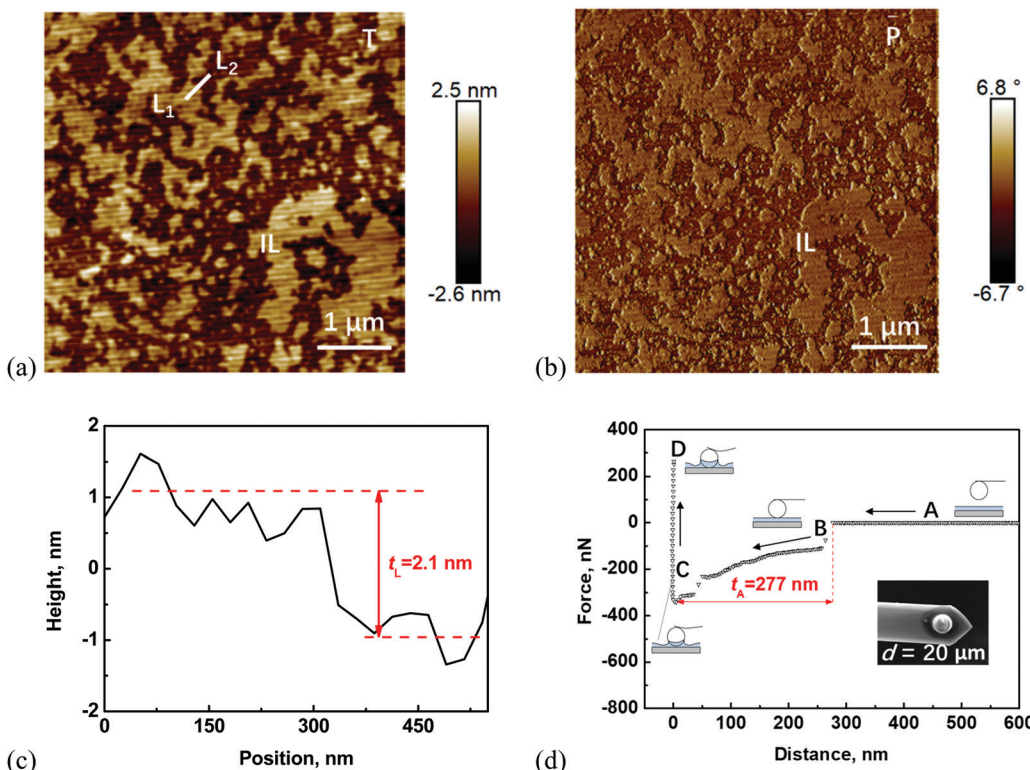


Fig. 1 AFM (a) topographical and (b) phase images of BB3-4-M, and (c) the corresponding cross-sectional profile along the line L_1L_2 in (a). T = topography, P = phase. (d) Representative force vs distance approaching curve and schematic of a glass colloidal microsphere at the end of a cantilever approaching the IL film on the mica surface (A–D, in the case of BB3-4-M), after contact, the microsphere being retracted (not shown here). The inset is a typical SEM image of a borosilicate glass microsphere (dimension, $d \sim 20 \mu\text{m}$) attached to a tipless silicon nitride cantilever. BB3-4-M means the IL film formed after a complete evaporation of ethanol by using 10^{-3} mL [BMIM][BF₄] IL per mL ethanol (4 μL) on the mica surface. t_L is the layering assembled ILs near the substrate, t_A is the apparent thickness including the assembled IL layers and the bulk.

acquired thickness from the difference in the height of the step (Fig. 1c) represents the film thickness of layering assembled ILs, t_L . The layering assembled ILs are the so-called solid phase of ILs, beneficial to the lubrication efficiency by preventing the direct substrate-to-substrate contact when generating normal forces.¹⁶

It is obvious that the thickness of layering assembled ILs at solid surfaces, t_L , does not show a monotonic increase or decrease with increasing amounts of the dropped ILs. Two questions arise: (1) What has changed at the IL–solid interfaces after varying the amounts of dropped ILs? (2) Do the ILs play any other role except for their contribution to the thickness of layering assembled ILs? We noted that the measured t_L is for the layering assembled ILs near the substrate, therefore, one possibility is that the rest of dropped ILs arrange further away from the substrate, and contributing to the bulk ILs. AFM approaching force–distance curve measured by colloidal probes was reported to directly infer the total film thickness of the ILs on solid substrates from the jump-in position.^{8,19,20} There are several technical requirements for the film thickness measurement *via* AFM colloidal probes: (1) the probe surface wetted by ILs with a strong capillary attraction, (2) the probe larger than the film thickness, to make sure the probe but not the whole cantilever is immersed in the IL, (3) a long cantilever is required so that the maximal cantilever deflection does not exceed a few

percent of its length.¹⁹ We thus attach borosilicate glass microspheres ($20 \mu\text{m}$ in dimension) to a tipless Cr–Au coated cantilever with a length of $110 \mu\text{m}$, and utilized the as-prepared AFM colloidal probe to capture the approaching force curves. A typical SEM image of an AFM colloidal probe (the dimension, $d \sim 20 \mu\text{m}$) is illustrated in the inset of Fig. 1d.

As shown in a typical approaching force curve of BB3-4-M in Fig. 1d, an AFM colloidal probe was moved toward the liquid film at the solid surface (A, B, C), and a steep linear force increase was observed in D, indicating that the contact had been established between the probe and the solid surface. The total film thickness of BB on mica can thus be obtained as 277 nm from the difference between the jump-in position of the piezo and the zero-force point on the contact line (horizontal double headed arrow in Fig. 1d), which is defined as the apparent thickness (t_A). Fig. S3 (ESI[†]) shows the approaching parts of typical force–distance curves recorded on other IL films at mica and HOPG substrates. As we expected, the increased amount of dropped IL solutions (10^{-5} mL ILs per mL ethanol, $1 \mu\text{L} \rightarrow 10^{-3}$ mL ILs per mL ethanol, 8 μL) onto $\sim 1 \text{ cm} \times 1 \text{ cm}$ solid surfaces, resulted in an increased apparent film thickness of ILs, t_A .

However, it is not clear if the thickness of the layering assembled ILs, t_L is included in this measured apparent

thickness, t_A . In the other word, the position of the probe contacts at zero separation might be the near-surface IL layers, rather than the solid substrate. As discussed previously by Atkin and Rutland *et al.*: it is possible that strongly adsorbed ILs resist squeeze-out even at high normal force, and the probe contacts an adsorbed IL layer rather than the solid surface at zero separation.^{28,29}

Black *et al.* have performed a series of force-distance measurements with increasing force set-points, to determine when the tip reaches the surface of the solid substrate. It was determined that the tip contacts the surface (zero separation is assigned to the surface) when no additional ion layers were observed in the IL with increasing the force set-point. However, they found that the force required to reach the surface is strongly dependent on the nature of AFM tips and ILs. If the cantilever is too stiff, it will not deflect when encountering an ion layer, and thus the ion layers cannot be detected, and the resulting force-curves become distorted. Softer cantilevers are ideal to monitor the structuring in ILs at solid interfaces due to their higher sensitivity to weak forces. However, if the cantilever is too soft, it may not be able to puncture through the ion layers to reach the surface. They collected force curves in an IL on mica using silicon nitride AFM probes (radius $\sim 50\text{--}60\text{ nm}$) with different spring constants ($0.66, 0.20$, and 0.09 N m^{-1}), and found only the probe with the spring constant of 0.20 N m^{-1} is able to detect the surface of mica.³⁰

We employed stiff cantilevers with spring constant of $\sim 8\text{ N m}^{-1}$ and a normal load of $\sim 1\text{ }\mu\text{N}$ for the force-distance curve measurements, and expected them to puncture through all ion layers to determine the total thickness of the formed IL film. No IL structuring was observed with these stiff cantilevers, consistent well with the observation by Black *et al.*,³⁰ but unlike them, our case did not show any distortions in the obtained force-curves. To confirm if the probe contacts the solid surface or the near-surface IL layer, we measured force-distance curves on the bare mica and HOPG surfaces with the same cantilevers that were used in IL-mica and IL-HOPG interfaces, as shown in Fig. S3 (ESI†). A steep linear increase in the force was observed at zero separation in both bare solid and IL-solid interfaces.

It is interesting that the slope of the linear regime in the bare mica substrate is almost the same as that in the IL-mica systems, and the same slope was also observed in the bare HOPG and IL-HOPG systems (Fig. S3, green dashed line, ESI†). This provides a hint that the stiffness of both the bare solid substrate and the IL-solid systems at zero separation is the same. Nevertheless, the same stiffness cannot ensure that the position the probe contacts at zero separation in IL-solid systems is the solid substrate, because the near-surface IL layers might be as stiff as the solid substrate. According to the AFM topography and phase images in Fig. 1 and Fig. S1 (ESI†), the near-surface IL layers exhibit apparently different elastic properties from the underlying solid substrate. This indicates the AFM probe-contacted position at zero separation in force curves of IL-solid systems is definitely the solid substrate, rather than the layering IL. Therefore, the film thickness of layering assembled ILs, t_L , is included in the apparent thickness, t_A .

3.2. Nanoscale frictional behavior of ILs on mica and HOPG substrates

Nanoscale friction of the ILs coated mica and HOPG substrates obtained using a silicon nitride AFM tip is shown in Fig. 2a and Fig. S4a, c, e (ESI†). The friction coefficient, μ , is determined from the gradient of the measured nanoscale friction and applied normal load in the linear regime. The observed nonzero intercepts with the vertical axis in the friction-load relationship is attributed to the adhesion force,^{31–33} arising mainly from van der Waals, electrostatic, and attractive capillary meniscus forces, *etc.*³⁴

As described in Sections 2.2 and 3.1, the ILs of different amounts were dropped on the substrates followed by complete evaporation of ethanol resulting in the ILs films of different apparent thicknesses. While the trends in friction coefficient data as shown in Fig. 2a and Fig. S4a, c, e (ESI†) seem to be independent of the apparent thickness, t_A . The friction coefficient, μ , for the bare mica and HOPG surfaces (thickness $\sim 0\text{ nm}$), are ~ 0.03 and 0.002 respectively. As indicated in Fig. 2a, we observed a slight reduction in the friction coefficient ($\mu = 0.029$) at a $\sim 12\text{ nm}$ thick IL BB on the mica substrate (BB5-1-M), while a

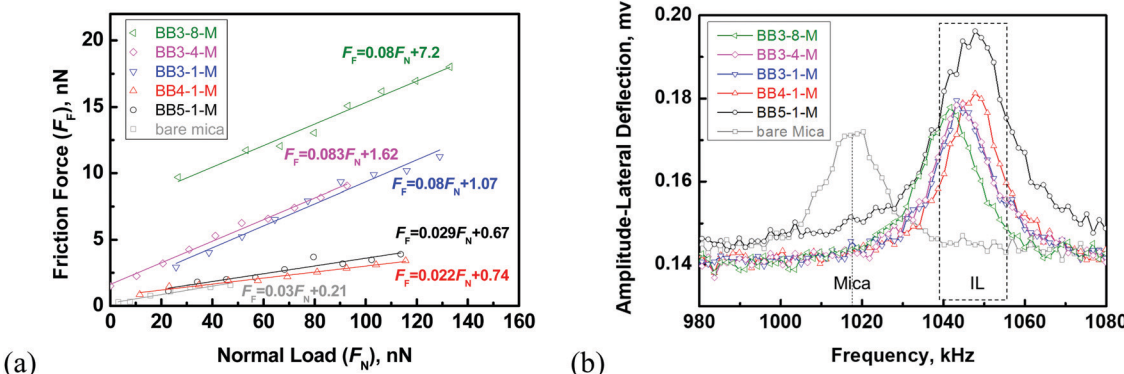


Fig. 2 (a) Typical friction force vs. applied normal load regressions used to calculate the friction coefficient, and (b) torsional resonance spectra from the lateral force signal, measured by rectangular silicon nitride cantilevers, for the bare mica and the BB IL on the mica surface at a normal load of $\sim 130\text{ nN}$. The slope in (a) is the friction coefficient μ , following the Amontons' friction law. BB5-1-M means the IL film formed after a complete evaporation of ethanol by using $10^{-5}\text{ mL [BMIM][BF}_4\text{] IL per mL ethanol (1 }\mu\text{L)}$ on the mica surface. The detail of the abbreviations is given in Table 1.

significantly reduced μ (0.022) was observed at ~ 54 nm thick film (BB4-1-M). As the film thickness of BB at the mica interface increased, it exhibited a dramatic increase in the friction coefficient: $\mu = 0.08, 0.083, 0.08$ for BB3-1-M, BB3-4-M, BB3-8-M, respectively. The addition of the BP IL onto the mica surface, enabled a significant increase in the friction coefficient, which revealed almost no dependence on the film thickness (Fig. S4e, ESI[†]).

In the friction measurements, a sharpened tip with a tip radius of 20 nm was used, so that the tip could penetrate the IL layers and get in a direct contact with the substrate. To ensure there is an IL film in the gap between the AFM tip and the substrate during friction measurements, we recorded the torsional resonance frequency at the highest applied normal load when measuring the friction force. The torsional resonance frequency is taken as a measure for the contact stiffness.^{35,36} The direct contact of the tip with the substrate must be established, as long as the contact stiffness on the IL coated substrate is the same as that on the bare substrate. It is observed clearly in Fig. 2b and Fig. S4b, d, f (ESI[†]), that the position of the resonance peak on the IL coated substrate shifts to a higher frequency relative to the bare substrate, indicating a completely different contact stiffness. This reflects the fact that the tip and the substrate are not in a direct contact when measuring the friction force even at the highest applied normal load.

3.3. Nanoscale friction versus the thickness of IL films at solid surfaces

As we discussed in Section 3.2, there is no dependence between the friction coefficient and the apparent thickness of ILs t_A , which has shown more clearly on the right panels in Fig. 3. Nevertheless, it is interesting to observe that the nanoscale friction coefficient μ increases monotonically as the layering thickness t_L decreases (left panels in Fig. 3). It should be noted that the friction coefficient remains approximately constant for an IL at a solid substrate which possesses the same layering thickness. For example, a constant friction coefficient was achieved over all of BP-mica cases because of their constant layering thickness ($t_L = \sim 2.5$ nm, left panels, Fig. 3b). Similar to our observations, Perkin's group also found an increased friction as the number of ion layers decreases, for the IL confined between two mica sheets. And they gave an explanation for the increased friction coefficient at a thinner IL layer: the layers closer to the mica surfaces are more ordered, with a greater ion excess concentration, resulting in a stronger 'inter-layer attraction' for the same value of contact area and a greater activation barrier for unlocking the surfaces to allow shear.¹⁵ However, Atkin's group^{37–39} found a different effect of the ordered IL layers on the friction coefficient: more ordered IL layers lead to smoother sliding plane and reduced friction coefficient, which also makes sense. Thus, it is a controversy over the effect of ordered IL layers on the friction coefficient at IL-solid interfaces, which is necessary to be investigated further.

Fig. 3 shows that the layering of IL ions could extend to tens of nanometers on the mica surface, in an agreement with the previous work,²³ because of the negative charge on mica

producing strong coulombic force between the IL and mica surface.⁴⁰ While thick extensive layers were not always observed on the charged mica surfaces,^{41,42} because the coulombic force depends on the structure of ILs.⁴³ For example, the IL, BB was found to form thinner IL layer on the mica than that on the HOPG in the cases of BB3-1, i.e., t_L is smaller in BB3-1-M than in BB3-1-H (left panels, Fig. 3a and c). Similarly, the IL, 1-ethyl-3-methylimidazolium acetate, formed 7 solvation layers on neutral HOPG surface, whereas the same IL has only 3 solvation layers on negatively charged mica surface.⁴¹ At this situation, coulombic force cannot be responsible for the extensive layers of the IL on HOPG, because HOPG surface has no charge, indicating that there must be other mechanisms.⁴⁰ The resulting different extensive layering thicknesses of ILs have a dramatic impact on the friction behavior.

The friction coefficient of ILs at the mica is higher than that at the HOPG surface, possibly due to the stronger interactions between the ILs and mica surface, which is due not only to the physical adsorption of ILs but also chemisorption via the formed N-Si bond between N-atom of the cation [BMIM]⁺ and Si-atom of the mica, as shown in XPS results in Fig. 4. The enhanced IL-mica interaction would result in more ordered IL layering at the mica surface, and thus higher friction, as proposed by Perkin *et al.*¹⁵

As for the lubrication mechanism, the typical Stribeck curve outlines lubrication regimes, namely hydrodynamic, mixed and boundary lubrication regimes. The role of ionic liquid-based lubricants is critically important in boundary lubrication regime. In general, the tribological surfaces used in real tribological applications are rough having many asperities and there is a direct contact between the asperities of the sliding surfaces and thus result in a higher friction. On the contrary, in the present work we employed mica and HOPG as the solid substrates which are smooth at the molecular scale (RMS = 0.66, 0.89 nm for mica and HOPG respectively) to ensure a single contact point. However, the link between the lubrication regimes (hydrodynamic, mixed, boundary lubrication) on a single asperity and the realistic motion is complex, because of the possible emergence of collective effects.⁴⁴ Therefore, a boundary regime with some contribution from the mixed regime was expected in our IL-solid systems.

Ionic liquids are charged lubricants and have the ability to form structured boundary layers on the surfaces mainly due to electrostatic interactions, leading to improved, 'intrinsic' boundary lubrication films.⁴⁵ SFA and AFM are two commonly used techniques to directly measure friction in the boundary lubrication regime, where the two solids are separated by a liquid film of a few molecules thickness on a single asperity.^{44,45}

In our IL-solid systems (Fig. 3), the AFM-measured friction coefficient increases monotonically as the thickness of the ordered IL layer (t_L , in the range of $\sim 2\text{--}14$ nm) decreases, no matter what the thickness of the bulk IL is. The friction coefficient remains essentially unchanged when the values of t_L are the same at a given IL-solid system, though the thicknesses of the bulk IL are differing. Thus, the assembled IL layers, rather than the bulk, determine the friction coefficient in our IL-solid systems, revealing that the lubrication mechanism does not belong to the

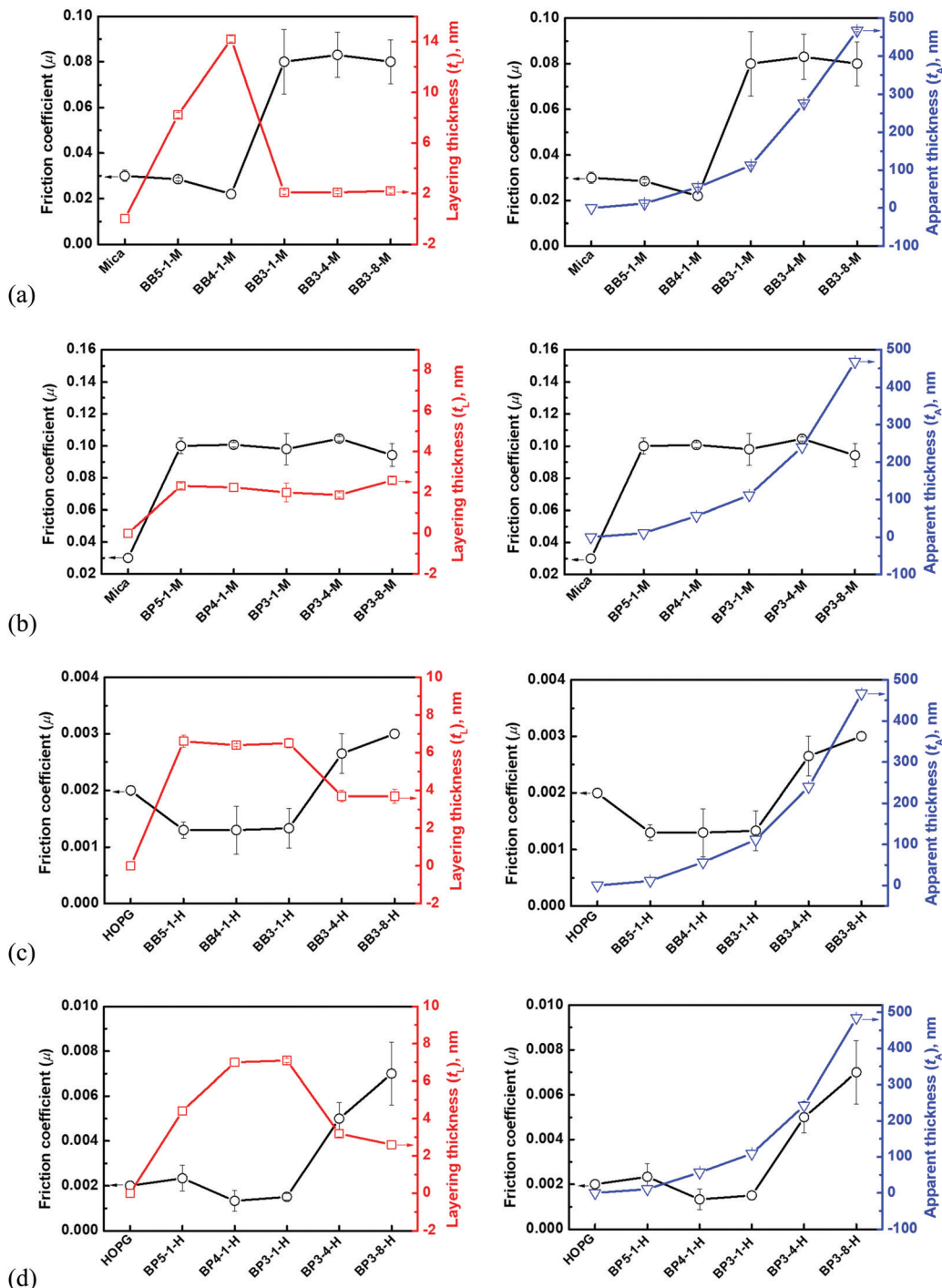


Fig. 3 Changes in the friction coefficient μ , layering thicknesses t_L (left panel), and apparent thickness t_A (right panel), of the IL films at mica and HOPG surfaces: (a) BB and (b) BP at mica surface; (c) BB and (d) BP at HOPG surface.

hydrodynamic regime. Furthermore, the torsional resonance frequency results at the highest applied normal load confirmed that the AFM probe slides on the top of the assembled IL layer during friction measurements. Overall, these observations reveal that the ILs act as intrinsic boundary lubricants in the present systems, due to their ability to bind to the surfaces and form surface layers with ordered structures to prevent a direct solid-to-solid contact.^{29,45}

Noting that some of IL–solid interfaces exhibit lower friction coefficient than the bare mica or HOPG substrates which are atomically flat. This implies that the assembled IL layers play an important role in reducing the nanoscale friction. While the obtained friction data are contributed by both the substrate and the layering ILs, rather than the latter only. Importantly, one could postulate that there are no changes in the structure and thickness of the assembled IL layers during the friction

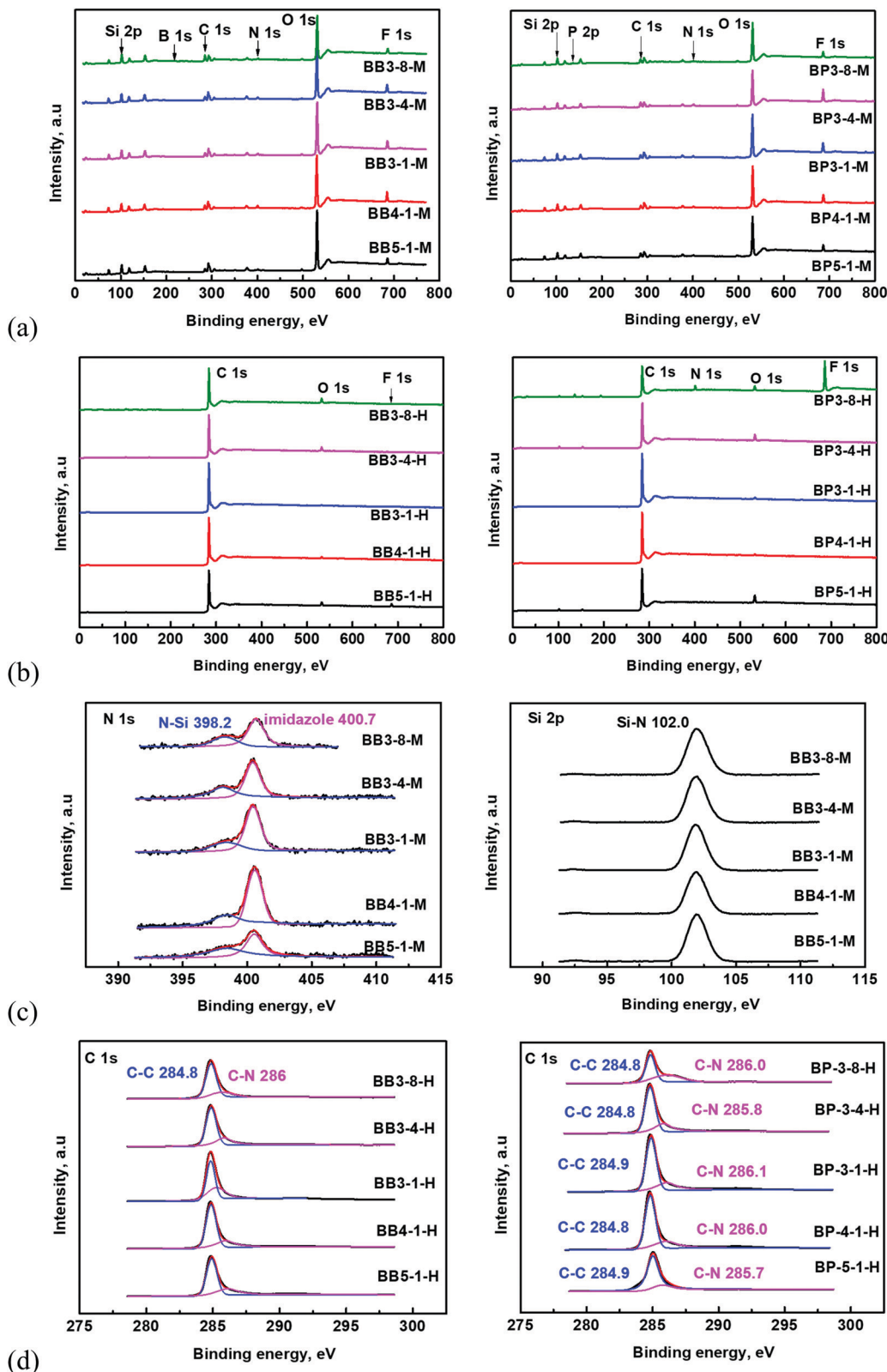


Fig. 4 Full XPS spectra of the ILs BB and BP on (a) mica and (b) HOPG surfaces, and high-resolution spectra of (c) Si 2p, N 1s at the BB–mica interfaces, and (d) C 1s at the BB–HOPG, BP–HOPG interfaces.

measurements. Because a concomitant abrupt increase should occur in friction, giving rise to a much higher friction coefficient,

if there is any squeeze-out of IL layers during the friction measurements. However, the nanoscale friction across the IL

layers on mica or HOPG surfaces were fitted as a linear function of the applied loads ($\sim 0\text{--}150$ nN), as shown in Fig. 3a and Fig. S4a, c, e (ESI†). We did not observe any abrupt change in the friction in the loading range, indicating that the applied highest loads in the present work are not sufficient to squeeze out the IL layers.

3.4. Interfacial behavior of IL films on mica and HOPG substrates

The assembled IL layers have been recognized as playing a central role in determining the interfacial friction coefficient relative to those of the bulk phase. What has changed at IL–solid interfaces? Since mica and HOPG substrates are the same for different IL systems, it is unlikely that there are topographical changes in the underlying substrates. We thus employed XPS further to examine the chemical changes at IL–solid interfaces to help in understanding the change in the friction coefficient with variations in the layering thickness, t_L .

Both XPS full and high-resolution spectra in Fig. 4 and Fig. S5 (ESI†) clearly reveal the presence of C, O, Si, N, B or P of BB and BP at the solid surfaces, and no significant changes were observed in binding energies as the layering or the apparent thickness changes. The high-resolution N 1s, F 1s, B 1s or P 2p spectra for the ILs at HOPG surfaces are not shown because of their low intensities. Especially for BB or BP coated mica surfaces, the XPS spectrum reveals a strong Si 2p peak at 102 eV assigned to the Si–N bond, and the binding energy of N 1s peak at 398.2 eV is attributed to N–Si bond¹⁵ (Fig. 4c and Fig. S5b, ESI†). This suggests that the imidazolium cation [BMIM]⁺ in BB or BP is strongly interacting with the negatively charged mica surface. It is evident that this interaction leads to not only the physical adsorption of ILs through electrostatic forces but also chemisorption *via* the formation of a covalent bond between N-atom of the cation [BMIM]⁺ and Si-atom of the mica.

However, we could not directly explain the interactive orientation of the ILs, BB or BP, on HOPG surfaces from the XPS spectra (Fig. 4d and Fig. S5a, ESI†). This is because that the HOPG

surface is composed only of carbon atoms, which also exist in the ILs. In a previous work by Yokota *et al.*⁴⁶ and Sha *et al.*,⁴⁷ the authors suggested preferential interactions of imidazolium ring of the cation [BMIM]⁺ with the graphite surface in the case of well-ordered ILs films at HOPG surface.

Noting that in the presence of water (humidity of $\sim 55\%$ during our friction measurements), the hydrolysis of both $[\text{BF}_4]^-$ and $[\text{PF}_6]^-$ anions might occur to form HF. To examine the occurrence of the hydrolysis, we performed XPS measurements for the neat ILs, [BB], [BP], and found the binding energy of 685.8 and 686.4 eV in F 1s spectra (Fig. S5c, ESI†) for $[\text{BF}_4]^-$ ⁴⁸ and $[\text{PF}_6]^-$ respectively.^{49,50} In comparison, at the prepared IL–solid interfaces, no shifts were observed in the characteristic bonds related to $[\text{BF}_4]^-$ or $[\text{PF}_6]^-$ (Fig. S5a and b, ESI†). This implies that only a negligible amount of HF is present (if produced, probably below the resolution of the XPS instrument). Therefore, the influence of the formed HF can be neglected.

3.5. IL distribution at solid–liquid interfaces

Typical XPS depth profiling analysis of BB3-1-M, BB3-4-M, BB3-8-M in Fig. 5, shows increasing N (from the [BMIM]⁺ cation), F (from the $[\text{BF}_4]^-$ anion) concentrations closer to the substrate surface and then revealing an almost constant level of elemental concentrations further away from the substrate. The observed N/F-rich layers near the BB–mica interface (~ 2 nm), indicate that the IL prefers to accumulating at the interface with more ordered layers, which is in accordance with the previous findings.¹⁵ While the fluctuations in the concentration of F in the region of $\sim >2$ nm from the substrate, reveal the IL disordering at a greater distance from the surface, and it is less stable than the IL adjacent to the substrate. The ~ 0 atomic concentration of N atoms at the position further than 2 nm from the substrate is due to the XPS detection limit.

Accordingly, it is understandable that the IL film on the substrate is composed of ordered (layering assembled ILs in the

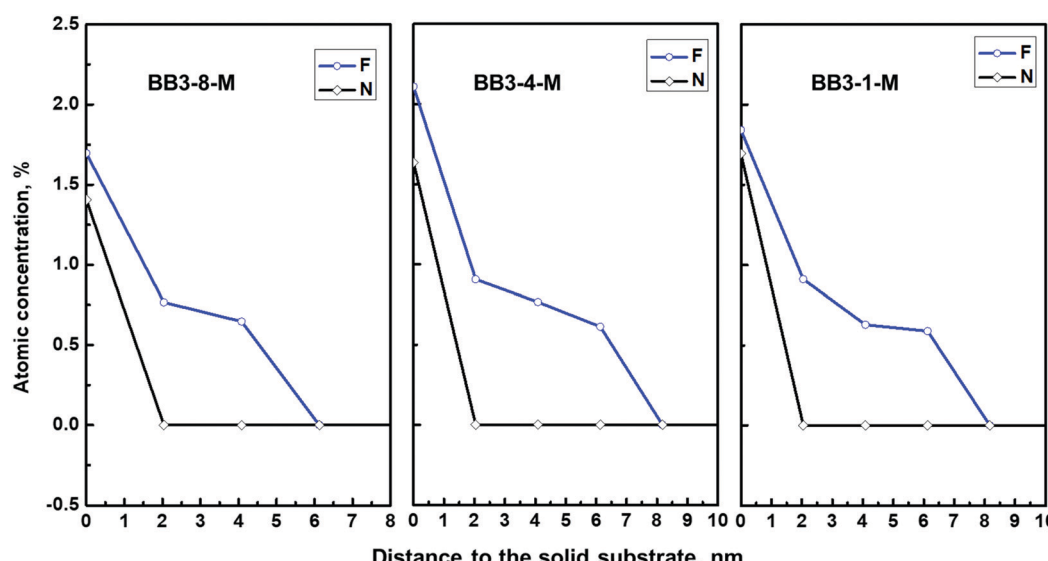


Fig. 5 XPS atomic concentration (%) depth profiles (F and N elements) at BB3-8-M, BB3-4-M, BB3-1-M interfaces.

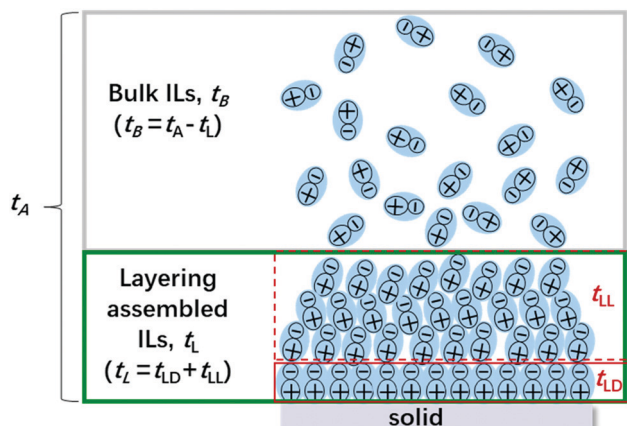


Fig. 6 Schematic illustration of IL films at solid–liquid interfaces. The layering assembled ILs are composed of dense and loose layers regimes, so the thickness of the near surface dense layer is referred as t_{LD} ; while the thickness of the upper slightly looser layer is t_{LL} .

green box, t_L) and/or disordered (bulk ILs in the grey box, t_B) ions forming on a solid substrate,¹⁵ as shown in the schematics in Fig. 6. As we discussed in Section 3.1, the apparent thickness of ILs, t_A , could be increased by increasing the amount of the dropped IL, but this controllable increase was observed not to hold for the layering thickness, t_L . A recent simulation work found the carbon slits confined IL to exhibit three-layered spatial distribution through number density profiles.⁵¹ They observed tighter packing and increased density of ions near the surface of a slit pore (dense layer), and a less prominent ion density peak at the position further away from the surface (sub-dense layer). However, no obvious density peak of ions was found at a greater distance from the surface, similar to the bulk phase.⁵¹ The proposed 3 distinct regions of ILs at the solid–liquid interfaces indicate that except for the bulk IL (t_B), the layering thickness of the IL, t_L , could be composed of two parts in our cases: (1) the IL adjacent to the solid substrate arranging in ordered layers (dense layer, t_{LD}), (2) the upper IL with decayed ordering into layers at a greater distance from the underlying solid surface (sub-dense layer), and we refer it as loose layer, t_{LL}), as illustrated in Fig. 6. We also observed triple layered IL confined between graphite and titanium dioxide slit pores in our ongoing simulation work for other type of ILs at solid surfaces. These data will be published elsewhere after through validation of the results.

Taking BB-mica as an example, at the smallest amount of IL addition, all the IL ions contributed to the formation of the assembled IL layer. As a consequence, the layering assembled IL thickness measured by AFM morphology is almost the same as that from approaching force–distance curves with AFM colloidal probes ($t_L = t_A \approx 12$ nm thick). As the amount of the IL increases, more IL ions joined the layering assembled IL, leading to a thicker ordered IL layer (BB4-1-M). While the ordering into layers decays at a greater distance from the surface, *i.e.*, it is less stable for the upper layering assembled IL as demonstrated by XPS depth profiling results shown in Fig. 5. Thus, the upper layering assembled IL (t_{LL}) was taken

away by the abundant bulk phase, resulting in a thinner ordered IL layer (BB3-1-M). The remaining IL layer interacts strongly with the underlying mica substrate, and thus preventing the ‘taken away’ by the bulk phase (Fig. 6). That is why a further increase of the IL amount has no influence on the thickness of the layering assembled IL (BB3-4-M, BB3-8-M). Therefore, the existence of loose layer of the IL, t_{LL} , determines the layering thickness, t_L , *i.e.*, t_L would be reduced if the upper loose layer is taken away by the abundant bulk IL. These measurements unveil an overlooked phenomenon, suggesting that further improvements of the lubricating performance can be sought at the scales dominated by the near-surface layering assembled IL.

4. Conclusions

We have compared the nanofriction characteristics of ILs on mica and HOPG surfaces at varying thicknesses. Well-defined IL films were achieved through drop-casting IL–ethanol dispersions and drying under vacuum. The increased amount of dropped ILs resulted in an increased apparent thickness of the IL films, which was measured directly from the jump-in distance in the AFM approaching force–distance curve with glass colloidal probes. While AFM morphologies showed that the ILs form extended layering structures with a completely different thickness from the measured apparent thickness. The apparent thickness, t_A , consists of 3 regions: (1) the IL adjacent to the solid substrate arranging in ordered layers (dense layer, t_{LD}), (2) the upper IL with decayed ordering into layers at a greater distance from the underlying solid surface (loose layer, t_{LL}), (3) the IL arranging further away from the substrate, contributing to the bulk phase (t_B).

The layering thickness of the extended IL, t_L , is composed of the dense (t_{LD}) and loose (t_{LL}) IL layers. While XPS depth profiling results demonstrated that the upper loose-layering assembled IL (t_{LL}) is less stable, which could be taken away by the abundant bulk phase, resulting in a thinner ordered IL layer and a smaller t_L . The layering assembled IL at solid surfaces has been found to be more important than the bulk phase in determining the magnitude of nanoscale friction, in which, the nanoscale friction coefficient (μ) increases monotonically as the layering thickness (t_L) decreases. For the IL that strongly interacts with a substrate, a decrease in the layering thickness means the ions are closer to the underlying surface. The closer ions are more ordered, resulting in a greater activation barrier for unlocking the surfaces to allow shear and thus provide a higher friction. These findings suggest that further improvements of the lubricating performance can be achieved at the scales dominated by the near-surface layering assembled ILs on the contact surfaces. The layering assembled IL with low friction coefficient, has a strong potential to allow for fast current transport,⁵² offering insights into the design principles for IL-based high-efficient energy conversion electrolytes.

Conflicts of interest

The authors declare no conflict of interest.

Acknowledgements

We are grateful to the support from the National Natural Science Foundation of China (Grant No. 21606131, 21838004, 21676137), Natural Science Foundation of Jiangsu Province (Grant No. BK20191289), and the financial support from Instrument & Equipment Open Funding of Nanjing University of Science and Technology. F. U. S. is grateful for the financial support of the Norrbotten Research Council (Grant No. NoFo 19-100).

References

- 1 F. Zhou, Y. Liang and W. Liu, *Chem. Soc. Rev.*, 2009, **38**, 2590–2599.
- 2 C. Ye, W. Liu, Y. Chen and L. Yu, *Chem. Commun.*, 2001, 2244–2245.
- 3 Y. Zhou and J. Qu, *ACS Appl. Mater. Interfaces*, 2017, **9**, 3209–3222.
- 4 H. Li, A. E. Somers, M. W. Rutland, P. C. Howlett and R. Atkin, *ACS Sustainable Chem. Eng.*, 2016, **4**, 5005–5012.
- 5 K. E. Gubbins, Y. Long and M. Śliwińska-Bartkowiak, *J. Chem. Thermodyn.*, 2014, **74**, 169–183.
- 6 R. An, L. Huang, Y. Long, B. Kalanyan, X. Lu and K. E. Gubbins, *Langmuir*, 2016, **32**, 743–750.
- 7 R. Hayes, G. G. Warr and R. Atkin, *Chem. Rev.*, 2015, **115**, 6357–6426.
- 8 S. Zhang, J. Zhang, Y. Zhang and Y. Deng, *Chem. Rev.*, 2017, **117**, 6755–6833.
- 9 F. Buchner, K. Förster-Tonigold, M. Bozorgchenani, A. Gross and R. J. Behm, *J. Phys. Chem. Lett.*, 2016, **7**, 226–233.
- 10 R. Hayes, G. G. Warr and R. Atkin, *Phys. Chem. Chem. Phys.*, 2010, **12**, 1709–1723.
- 11 M. A. Gebbie, A. M. Smith, H. A. Dobbs, A. A. Lee, G. G. Warr, X. Banquy, M. Valtiner, M. W. Rutland, J. N. Israelachvili, S. Perkin and R. Atkin, *Chem. Commun.*, 2017, **53**, 1214–1224.
- 12 X. Gong, A. Kozbial and L. Li, *Chem. Sci.*, 2015, **6**, 3478–3482.
- 13 A. Sheehan, L. A. Jurado, S. N. Ramakrishna, A. Arcifa, A. Rossi, N. D. Spencer and R. M. Espinosa-Marzal, *Nanoscale*, 2016, **8**, 4094–4106.
- 14 R. An, L. Huang, K. P. Mineart, Y. Dong, R. J. Spontak and K. E. Gubbins, *Soft Matter*, 2017, **13**, 3492–3505.
- 15 A. M. Smith, K. R. J. Lovelock, N. N. Gosvami, T. Welton and S. Perkin, *Phys. Chem. Chem. Phys.*, 2013, **15**, 15317–15320.
- 16 J. Comtet, A. Niguès, V. Kaiser, B. Coasne, L. Bocquet and A. Siria, *Nat. Mater.*, 2017, **16**, 634.
- 17 W. Liu, K. Bonin and M. Guthold, *Rev. Sci. Instrum.*, 2007, **78**, 063707.
- 18 R. Lhermerout and S. Perkin, *Phys. Chem. Chem. Phys.*, 2020, **22**, 455–466.
- 19 J. Ally, E. Vittorias, A. Amirkazli, M. Kappl, E. Bonaccorso, C. E. McNamee and H.-J. Butt, *Langmuir*, 2010, **26**, 11797–11803.
- 20 B. Bhushan, J. N. Israelachvili and U. Landman, *Nature*, 1995, **374**, 607–616.
- 21 Z. Wang and C. Priest, *Langmuir*, 2013, **29**, 11344–11353.
- 22 Y. Liu, Y. Zhang, G. Wu and J. Hu, *J. Am. Chem. Soc.*, 2006, **128**, 7456–7457.
- 23 S. Bovio, A. Podestà, C. Lenardi and P. Milani, *J. Phys. Chem. B*, 2009, **113**, 6600–6603.
- 24 X. Gong, B. Wang and L. Li, *ACS Omega*, 2018, **3**, 16398–16402.
- 25 X. He, C. Wu, K. Rajagopal, N. Punpongjareorn and D.-S. Yang, *Phys. Chem. Chem. Phys.*, 2016, **18**, 3392–3396.
- 26 A. J. Page, A. Elbourne, R. Stefanovic, M. A. Addicoat, G. G. Warr, K. Voitchovsky and R. Atkin, *Nanoscale*, 2014, **6**, 8100–8106.
- 27 J. Melcher, C. Carrasco, X. Xu, J. L. Carrascosa, J. Gómez-Herrero, P. José de Pablo and A. Raman, *Proc. Natl. Acad. Sci. U. S. A.*, 2009, **106**, 13655–13660.
- 28 H. Li, F. Endres and R. Atkin, *Phys. Chem. Chem. Phys.*, 2013, **15**, 14624–14633.
- 29 O. Werzer, E. D. Cranston, G. G. Warr, R. Atkin and M. W. Rutland, *Phys. Chem. Chem. Phys.*, 2012, **14**, 5147–5152.
- 30 J. M. Black, M. Zhu, P. Zhang, R. R. Unocic, D. Guo, M. B. Okatan, S. Dai, P. T. Cummings, S. V. Kalinin, G. Feng and N. Balke, *Sci. Rep.*, 2016, **6**, 32389.
- 31 B. Quignon, G. A. Pilkington, E. Thormann, P. M. Claesson, M. N. R. Ashfold, D. Mattia, H. Leese, S. A. Davis and W. H. Briscoe, *ACS Nano*, 2013, **7**, 10850–10862.
- 32 A. M. Smith, K. R. Lovelock, N. N. Gosvami, T. Welton and S. Perkin, *Phys. Chem. Chem. Phys.*, 2013, **15**, 15317–15320.
- 33 Y. Leng and S. Jiang, *J. Am. Chem. Soc.*, 2002, **124**, 11764–11770.
- 34 J. B. Pethica and W. C. Oliver, *Phys. Scr.*, 1987, 61.
- 35 U. Rabe, S. Amelio, E. Kester, V. Scherer, S. Hirsekorn and W. Arnold, *Ultrasonics*, 2000, **38**, 430–437.
- 36 S. Maier, Y. Sang, T. Filletter, M. Grant, R. Bennewitz, E. Gnecco and E. Meyer, *Phys. Rev. B: Condens. Matter Mater. Phys.*, 2005, **72**, 245418.
- 37 H. Li, M. W. Rutland and R. Atkin, *Phys. Chem. Chem. Phys.*, 2013, **15**, 14616–14623.
- 38 P. K. Cooper, C. J. Wear, H. Li and R. Atkin, *ACS Sustainable Chem. Eng.*, 2017, **5**, 11737–11743.
- 39 H. Li, M. W. Rutland, M. Watanabe and R. Atkin, *Faraday Discuss.*, 2017, **199**, 311–322.
- 40 X. Gong, A. Kozbial, F. Rose and L. Li, *ACS Appl. Mater. Interfaces*, 2015, **7**, 7078–7081.
- 41 R. Atkin and G. G. Warr, *J. Phys. Chem. C*, 2007, **111**, 5162–5168.
- 42 A. Deyko, T. Cremer, F. Rietzler, S. Perkin, L. Crowhurst, T. Welton, H.-P. Steinrück and F. Maier, *J. Phys. Chem. C*, 2013, **117**, 5101–5111.
- 43 M. A. Gebbie, M. Valtiner, X. Banquy, E. T. Fox, W. A. Henderson and J. N. Israelachvili, *Proc. Natl. Acad. Sci. U. S. A.*, 2013, **110**, 9674–9679.
- 44 R. Lhermerout, C. Diederichs and S. Perkin, *Lubricants*, 2018, **6**, 9.
- 45 N. Hjalmarsson, R. Atkin and M. W. Rutland, *Phys. Chem. Chem. Phys.*, 2016, **18**, 9232–9239.
- 46 Y. Yokota, T. Harada and K.-I. Fukui, *Chem. Commun.*, 2010, **46**, 8627–8629.
- 47 S. Maolin, Z. Fuchun, W. Guozhong, F. Haiping, W. Chunlei, C. Shimou, Z. Yi and H. Jun, *J. Chem. Phys.*, 2008, **128**, 134504.

- 48 S. Bai, P. Da, C. Li, Z. Wang, Z. Yuan, F. Fu, M. Kawecki,
X. Liu, N. Sakai, J. T.-W. Wang, S. Huettner, S. Buecheler,
M. Fahlman, F. Gao and H. J. Snaith, *Nature*, 2019, **571**,
245–250.
- 49 D. Ensling, M. Stjerndahl, A. Nyten, T. Gustafsson and
J. O. Thomas, *J. Mater. Chem.*, 2009, **19**, 82–88.
- 50 T. Morishita and N. Takahashi, *RSC Adv.*, 2017, **7**, 36450–36459.
- 51 Z. Dai, Y. You, Y. Zhu, S. Wang, W. Zhu and X. Lu, *J. Phys.
Chem. B*, 2019, **123**, 6857–6869.
- 52 P. Brown, X. Mao, C. Cervinka, G. Hazell, H. Li, Y. Ren,
D. Chen, R. Atkin, J. Eastoe, I. Grillo, A. Pádua, M. Gomes
and T. Hatton, *Nat. Mater.*, 2019, **18**, 1350–1357.